Supporting Information:

Nature of the active sites for CO reduction on copper nanoparticles; suggestions for optimizing performance

*Tao Cheng, Hai Xiao, and William A Goddard III**

Materials and Process Simulation Center (MSC) and Joint Center for Artificial Photosynthesis (JCAP), California Institute of Technology, Pasadena, California 91125, United States

* E-mail: wag@wag.caltech.edu

S1 simulation methods

We used LAMMPS (1 Feb 2014 version)[1] with the USER-REAXC package and fix qeq/reax.[2] for the Molecular Mechanics (MM) Dynamics simulations. A Nose-Hoover thermostat was used to control the temperature with a damping parameter of 100 time steps.

To grow a copper (Cu) nanoparticle (NP), we used a zigzag carbon nanotube (CNT) with a diameter of 8.39 nm as the catalysis support, which was kept fixed during all the simulations. The Embedded-atom-model (EAM) was used to describe the interaction between Cu atoms,[3] and a Lennard-Jones (LJ) potential was used to describe the interaction between Cu and the CNT. The temperature for the growth simulation was 300K, and the deposition rate for the growth simulation was 3.2Å ns^{-1}. The time step was 1 fs. After 30 ns of growth simulation, a Cu NP with a normal thickness of about 10 nm was obtained on the CNT support. Annealing simulations were carried out to heal the defect and increase the grain size. Each annealing cycle included 10 ps cook-off simulation from 300 K to 1200 K, 5 ps NVT simulation at 1200 K, 10 ps annealing from 1200 K to 300 K and 15 ps NVT simulation at 300 K. After 100 annealing cycles, a fully crystallized Cu NP formed on CNT support. In the annealing trajectory, the Cu-NP structure after 36 annealing cycles is mostly close to the experimental structure, which was further refined by using 20 ps ReaxFF reactive force field (ReaxFF) simulation at 300K. The time step for the reactive force field (ReaxFF) simulations was 0.25 fs.

Quantum mechanics calculations were performed with VASP package [4-6], using the PBE flavor[7] of DFT and the projector augmented wave (PAW) method[8] to account for core-valence interactions. The kinetic energy cutoff for plane wave expansions was set to 400 eV. The Methfessel-Paxton smearing of second order with a width of 0.2 eV was applied. The convergence criteria are 1×10^{-5} eV energy differences for solving the electronic wavefunction. All geometries (atomic coordinates) are converged to 1×10^{-2} eV/Å for maximal components of forces. In calculations of periodic surfaces, we used 3x3x4 Cu (100) surface, 3x3x4 Cu(111) surface and 3x3x4 Cu(211) surface with experimental lattice parameters. The bottom two layers were fixed in the calculation with vacuum layers of at least 15 Å. Reciprocal space was sampled by the Γ-centered Monkhorst-Pack scheme with a grid of 3×3×1. For cluster calculations, a 20 Å cubic box was used, and only gamma point was considered in these calculations. All the Cu atoms were fixed in cluster calculations.

The binding energy of CO is (E_{binding}) calculated as follows:

$$E_{\text{binding}} = E_{*\text{CO}} - (E_{*} + E_{\text{CO}}) \tag{S1}$$

The formation energy of *OCCOH ($E_{*\text{OCCOH}}^{\text{Formation}}$) is calculated as follows:

$$E_{*\text{OCCOH}}^{\text{Formation}} = E_{*\text{OCCOH}} - (E_{*\text{CO}+*\text{CO}} + \frac{E_{\text{H}_2}}{2}) \tag{S2}$$

Debyer, (freely available on https://github.com/wojdyr/debyer), was used to calculate the diffraction pattern for the synchrotron x-ray source. QSTEM (freely available on http://qstem.org/) was used to simulate the TEM images.

S2 validation of the ReaxFF

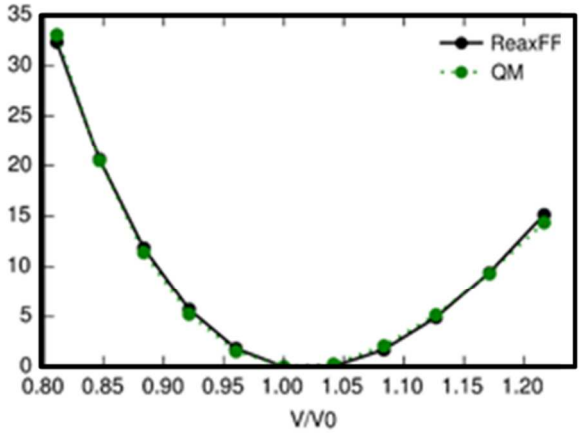

Figure S1. Comparison of the equation of state of Copper (FCC) between reaxFF and QM (DFT PBE).

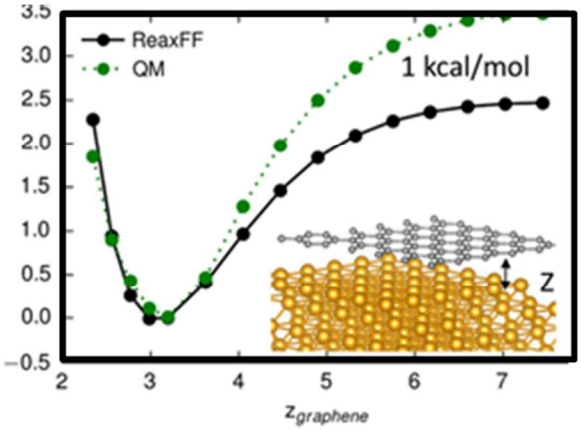

Figure S2. Comparison of binding energy of single layer graphene and Cu(111) surface between reaxFF and QM (DFT PBE).

S3 Binding Energy Calculations

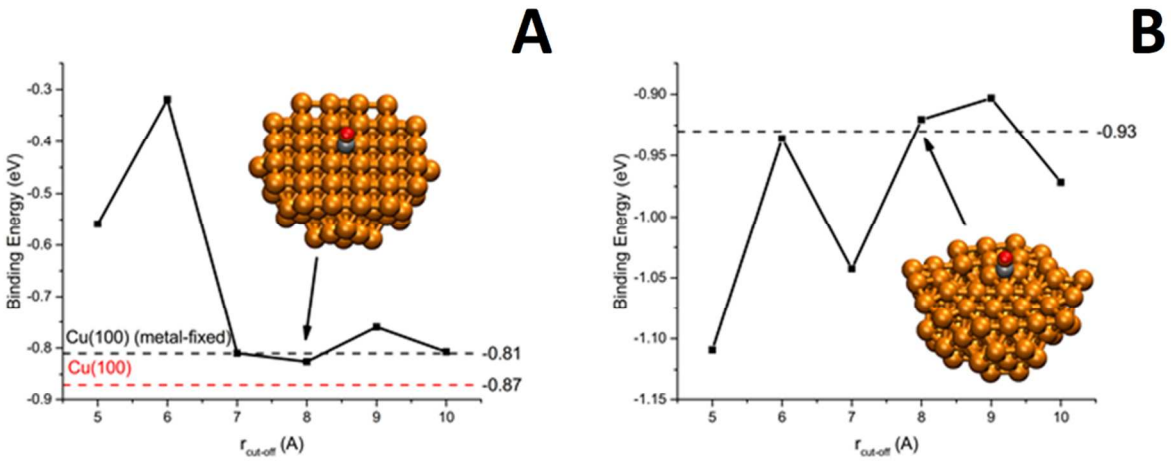

Figure S3. (A) The potential energy convergence benchmark as a function of cut-off radius for Cu(100) surface. (B) The potential energy convergence benchmark as a function of cut-off radius for an amorphous Cu surface.

As shown in Figure S3, the largest cut-off radius is 10 Å in these benchmark calculations. Our results show that 8.0 Å is already sufficient to converge the energy to within 0.02 eV. Therefore, we consider that 8.0 Å provides the right balance of accuracy and efficiency. Thus, we use this cut-off throughout our work. The number of atoms in the QM cluster calculations varied between 80 and 100, depending on the local environment of the selected site.

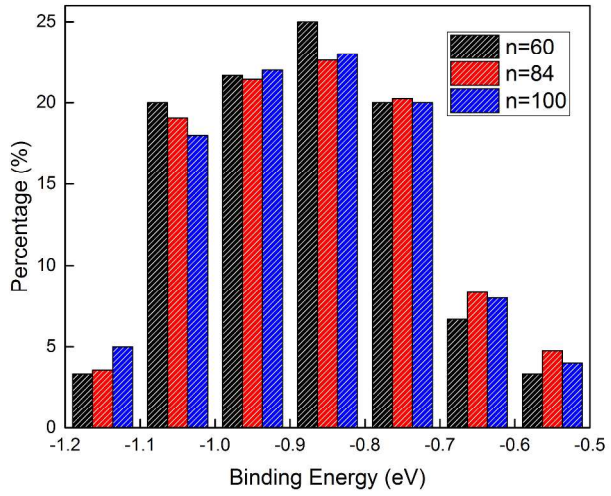

Figure S4. The distribution of CO binding energies (eV) from sampling with n = 60, 84 and 100 randomly selected surface sites.

As shown in the Figure S4, we compared the CO binding energy distributions from three sets of data: n = 60, n = 84 and n = 100. All these three data sets show similar statistical distributions, but smaller fluctuations as the set size increases.

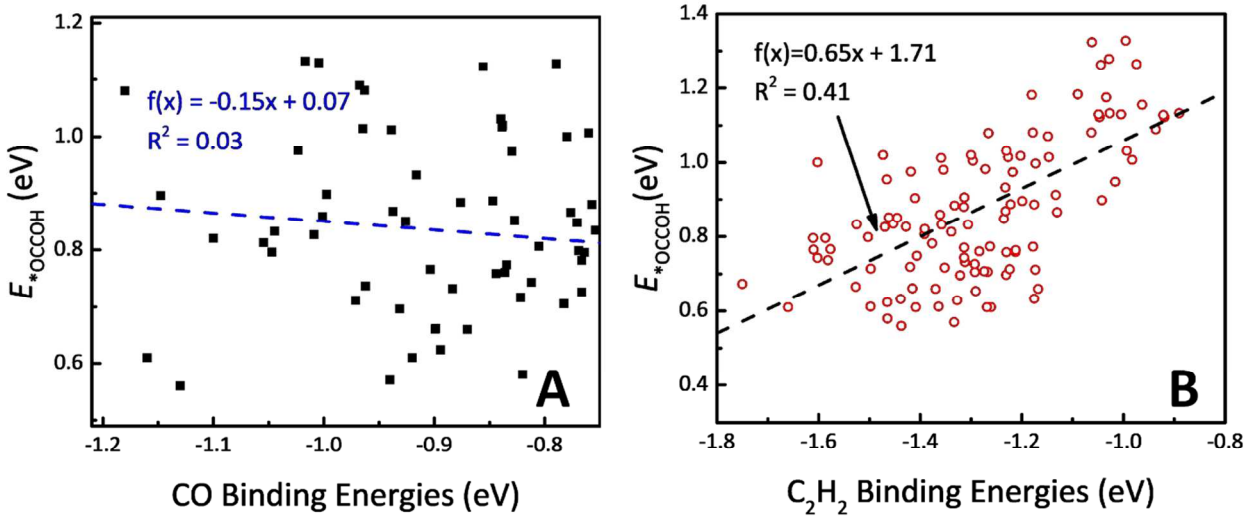

Figure S5. The formation energies of *OCCOH (E_{*OCCOH}, in eV) versus (A) CO binding energies (in eV), and (B) C_2H_2 binding energies (in eV). Note that half of the 4 best CO binding sites lead to low barriers for *OCCOH and that the two best C_2H_2 binding sites both lead to low barriers for *OCCOH.

As shown in Figure S5A, the distribution of energies for forming the *OCCOH (E_{*OCCOH}) have no apparent correlation (R^2 = 0.03) with *CO binding energies. This lack of correlation may be explained by the following reasons:

i. *CO and *OCCOH have a different preference for surface sites. For example, step sites might increase *CO binding but not *OCCOH binding.

ii. *CO binding requires one surface site, but *OCCOH formation is always from two *CO, which requires two surface sites. Therefore, to promote *OCCOH formation, the best solution is to combine one strong site and one weak site (instead of two strong sites). However, the random distribution of surface sites on NPs cannot guaranty that a strong site accompanies with a weak site, which can only be achieved by rational design as we proposed at the end of the manuscript.

As shown in Figure S5A, the distribution of energies for forming the *OCCOH (E_{*OCCOH}) have no overall correlation (R^2 = 0.03) with *CO binding energies. However, of the 4 best CO binders, two have low OCCOH binding, as discussed in the text. The binding energies of C_2H_2 exhibit better correlations with E*OCCOH, although the correlation is still far from significant (R^2=0.41). However, the best two for C_2H_2 binders do give lower formation energies for CC coupling. Thus C_2H_2 is a better probe molecule than *CO.

Although *OCCOH (E_{*OCCOH}) have no apparent correlation with *CO binding energies in the overall sites investigated, the population of active sites among CO binding sites stronger than -1.07 eV is high, ~50% (2/4). In contrast, the population of active sites among all strong CO binding sites (less than -1.07 eV) is only 3.75% (3/80). Therefore, it is much easier to locate active sites among the ensemble of strong CO binding sites, which is our strategy to discover active sites efficiently.

We consider that strong *OCCOH binding is a good descriptor for sites that do C-C coupling. However, theoretical screening using *OCCOH is much more expensive than screening using *CO, because with *OCCOH we must consider many more possible orientations. In contrast *CO is easy to calculate. Thus, basing on our calculations we estimated that *OCCOH screening is about ten times slower than *CO calculations. Therefore, we recommend doing the first round of *CO scanning to locate the strong CO binding sites, followed by a second round of *OCCOH calculation for a much smaller group of possible sites (four in this work).

S4 ReaxFF parameters

```
2017-04-01 23:39:22 : C|Cu
 39
   50.0000
    5.5469
   21.2839
    3.0000
    6.5000
    1.0000
    1.0159
    9.0000
    8.0878
   13.0238
  -13.8107
    0.0000
   10.0000
    2.8793
   33.8667
   25.6125
    1.0563
    2.0384
    6.1431
    6.9290
    0.3989
    3.9954
   -2.4837
    4.7747
   10.0000
    2.3276
   -1.2327
    2.1645
    1.5591
    0.1000
    2.8921
    1.6356
    5.6937
    2.5067
    0.5000
   20.0000
    5.0000
    0.0000
    1.6052
 2    ! Nr of atoms; cov.r; valency;a.m;Rvdw;Evdw;gammaEEM;cov.r2;#
           alfa;gammavdW;valency;Eunder;Eover;chiEEM;etaEEM;n.u.
           cov r3;Elp;Heat inc.;n.u.;n.u.;n.u.;n.u.
           ov/un;val1;n.u.;val3,vval4
 C    1.3460   4.0000  12.0000   1.6535   0.0700   0.8712   1.3405   4.0000
      9.9851   2.3853   4.0000  37.7798  75.7665   5.7254   6.9235   0.0000
      1.1961   0.0000 206.7910   5.0966  26.6796  13.0315   0.8563   0.0000
   -15.2102   2.4601   1.0564   6.2998   2.9663   0.0000   0.0000   0.0000
 Cu   2.0072   1.0000  63.5460   1.8672   0.1976   0.8218  -1.0000   1.0000
     11.6434   5.9108   1.0000   0.0000   0.0000   1.8038   7.3852   0.0000
     -1.0000   0.0000  92.5070   6.2292   5.3864   0.1573   0.8563   0.0000
     -1.9334   2.9867   1.0338   6.2998   2.5791   0.0000   0.0000  99.9916
 3      ! Nr of bonds; Edis1;LPpen;n.u.;pbe1;pbo5;13corr;pbo6
                       pbe2;pbo3;pbo4;n.u.;pbo1;pbo2;ovcorr
  1  1 143.7906 120.4394  65.4867   0.0698  -0.3990   1.0000  17.5908   0.5000
         0.1473  -0.2351   8.2239   1.0000  -0.1232   6.4008   1.0000   0.0000
  1  2   0.0000   0.0000   0.0000   0.1090  -0.2194   1.0000  15.3718   0.5191
         0.7294  -0.2364   8.3959   1.0000  -0.0920   7.3348   1.0000   0.0000
  2  2  71.8541   0.0000   0.0000   0.0004  -0.2000   0.0000  16.1600   0.3324
```

```
        0.9311  -0.2060  14.9286   1.0000  -0.1050   5.9705   0.0000   0.0000
1    ! Nr of off-diagonal terms; Ediss;Ro;gamma;rsigma;rpi;rpi2
 1  2   0.1116   1.9801  10.2733   1.2613   1.3494  -1.0000
3    ! Nr of angles;at1;at2;at3;Thetao,o;ka;kb;pv1;pv2
 1  1  1  75.3892  20.0233   2.1017   2.4996   0.0031  35.9933   1.0400
 1  2  1  78.5349  24.8509   1.7087   0.0000   0.7675   0.0000   1.2475
 1  1  2  44.4872   5.9709   1.9229   0.0000   0.0221   0.0000   1.1759
6    ! Nr of torsions;at1;at2;at3;at4;;V1;V2;V3;V2(BO);vconj;n.u;n
 1  1  1  2   0.0000   0.0000   0.0000   0.0000   0.0000   0.0000   0.0000
 1  2  1  1   0.0000   0.0000   0.0000   0.0000   0.0000   0.0000   0.0000
 2  1  1  2   0.0000   0.0000   0.0000   0.0000   0.0000   0.0000   0.0000
 1  2  1  2   0.0000   0.0000   0.0000   0.0000   0.0000   0.0000   0.0000
 2  2  1  1   0.0000   0.0000   0.0000   0.0000   0.0000   0.0000   0.0000
 1  2  2  1   0.0000   0.0000   0.0000   0.0000   0.0000   0.0000   0.0000
 0    ! Nr of hydrogen bonds;at1;at2;at3;Rhb;Dehb;vhb1
```

References

1. Plimpton, S., *J. Comput. Phys.* **1995,** *117*, 1-19.
2. Aktulga, H. M.; Fogarty, J. C.; Pandit, S. A.; Grama, A. Y., *Parallel Comput* **2012,** *38*, 245-259.
3. Foiles, S. M.; Baskes, M. I.; Daw, M. S., *Phys. Rev. B: Condens. Matter Mater. Phys.* **1986,** *33*, 7983-7991.
4. Kresse, G.; Hafner, J., *Phys. Rev. B: Condens. Matter Mater. Phys.* **1993,** *47*, 558-561.
5. Kresse, G.; Furthmüller, J., *Comput. Mater. Sci.* **1996,** *6*, 15-50.
6. Kresse, G.; Furthmüller, J., *Phys. Rev. B: Condens. Matter Mater. Phys.* **1996,** *54*, 11169-11186.
7. Perdew, J. P.; Burke, K.; Ernzerhof, M., *Phys. Rev. Lett.* **1996,** *77*, 3865-3868.
8. Kresse, G.; Joubert, D., *Phys. Rev. B: Condens. Matter Mater. Phys.* **1999,** *59*, 1758-1775.